

02,05,12

Structural Properties of Nb/Dy and Nb/Ho Superlattices

© V.D. Zhaketov^{1,3,6}, D.I. Devyaterikov², M.M. Avdeev^{1,3}, D.A. Norov^{1,3}, E.D. Kolupaev^{1,3}, M.O. Kuzmenko¹, N.G. Pugach⁴, Yu.N. Khaydukov³, E.A. Kravtsov^{2,5}, Yu.V. Nikitenko¹, V.L. Aksenov¹

¹ Joint Institute for Nuclear Research, Moscow oblast, Dubna, Russia

² M.N. Mikheev Institute of Metal Physics, Ural Branch, Russian Academy of Sciences, Yekaterinburg, Russia

³ Lomonosov Moscow State University, Moscow, Russia

⁴ National Research University Higher School of Economics, Moscow, Russia

⁵ Ural Federal University after the first President of Russia B.N. Yeltsin, Yekaterinburg, Russia

⁶ Moscow Institute of Physics and Technology, Dolgoprudny, Russia

E-mail: zhaketov@nf.jinr.ru

Received April 17, 2023

Revised April 17, 2023

Accepted May 11, 2023

Proximity effects in structures with helimagnetic ordering are investigated. Structures with sharp boundaries were prepared by magnetron sputtering. Results indicating a change in the magnetic state of a helimagnet under the influence of superconductivity were obtained by polarized neutron reflectometry. A new type of structure with alternating layers of a superconductor and a rare-earth helimagnet is proposed for studying magnetic proximity effects. The results of studies using X-ray methods and atomic force microscopy demonstrate the high quality of the obtained structures.

Keywords: helimagnetism, superconductivity, heterostructures, superlattices, neutron reflectometry.

DOI: 10.61011/PSS.2023.07.56393.35H

1. Introduction

Proximity effects at an interface are currently extensively studied. Of particular interest are two-dimensional low-scale structures with superconducting (S) and ferromagnetic (F) properties where interaction of two mutually antagonistic order parameters [1–3] is implemented. The signs of ferromagnetism effects influencing the superconducting properties of S/F heterostructures include phase changes of the superconducting order parameter (π -phase superconductivity) and spin-triplet cooper pairing. Less attention is paid to the investigation of inverse proximity effects when superconductivity affects ferromagnetism [4–6]. Such magnetic proximity effects are expected in the systems where the ferromagnetic and superconducting transition temperatures are comparable. Niobium and rare-earth (RE) metal S/F heterostructures are promising systems for the investigation of proximity effects [7,8]. High transparency of S/F interface is primarily noted for such RE/Nb systems as Gd/Nb, which simplifies penetration of superconducting correlations in F layers. Second, rare-earth metals are characterized by low ferromagnetism, which makes the energies of both interactions closer and simplifies the implementation of proximity effects. Third, some rare earth elements such as Dy and Ho are rare-earth antiferromagnetic

materials with helicoidal structure allowing to generate long-range triplet superconductivity.

The helicoidal magnetic structure is formed in bulk Dy in the interval between the Curie temperature ($T_F = 85$ K) and Neel temperature ($T_N = 178$ K), in bulk Ho in the interval between $T_F = 18$ K and $T_N = 132$ K. Due the effect of dimensional effects and epitaxial stresses in low-dimensional Dy- and Ho-based heterostructures, the magnetic structure shows peculiarities such as the Curie and Neel temperature variation and different helicoid periods compared with bulk materials. Thin Dy(200 nm) and Ho(200 nm) films and [Dy(6 nm)/Ho(6 nm)] superlattices were studied [9–12]. Phase transition temperature variation, e.g. decreasing Curie temperature in thin Dy film (200 nm), was shown. Note that the possibility of creating spin valves based on such structures is addressed in [13–15]. In [16], three-layer Ho/Nb/Ho and Dy/Nb/Dy systems were investigated and the superconducting transition temperature was shown to differ by 400 mK in cases of zero magnetic field and applied magnetic field in the structure plane. Inverse effects associated with helimagnet state variation under the influence of superconductivity have not been ever investigated. The aim of this study was to carry out such investigation for the first time. The primary objective of the study was to detect magnetic state variation in the periodic structure [Dy/Ho]

sputtered on the buffer layer of superconducting niobium. This structure was made for the study of mutual influence of two different Dy and Ho helimagnetics in a low-dimensional system, but in [9], magnetic helicoid periods in Dy and Ho layers in [Dy(6 nm)/Ho(6 nm)] superlattices are reported to exceed the helicoid periods for bulk Dy and Ho due to dimensional effects. The study includes more detailed review of low-temperature measurements obtained for this structure at a temperature below $T_c(\text{Nb})$. The second objective of the study was to offer better periodic structures with alternating superconducting and helimagnetic layers with the necessary parameters. In [7], periodic Nb/Gd structures were studied, thin ferromagnetic Gd layers with thicknesses approximately equal and lower than the correlation superconductivity length in ferromagnetic material $\xi_F(\text{Gd}) = 4 \text{ nm}$, were located between $d(\text{Nb}) = 25 \text{ nm}$ superconducting layers. In such approach, superconducting correlations penetrate ferromagnetic layers. The study suggests that the rare earth element and superconducting Nb interface is characterized by a low rms roughness amplitude of max. 1 nm, layer thickness deviation from nominal values is max. 10%. This property of structures allowed to investigate the proximity effects, diamagnetism of periodic ferromagnetic superconducting Nb/Gd structure at a temperature below the superconducting critical temperature. Within this study, periodic Nb/Dy and Nb/Ho structures with similar thicknesses described in [7] were made. The objective was to identify the parameters and quality of the obtained structures. Further study will perform neutron characterization of these systems.

Note that the benefit of the multilayer structures with helicoidal/fan-shaped magnetization studied herein compared with the multilayer structures from the alternating ferromagnetic layers with noncollinear magnetization and thick ferromagnetic layers (Ho and Dy) with helicoidal magnetization. In the first case, the disadvantages are, first, that noncollinear magnetization varies on a much greater length than the helicoid period $d_{he} \approx 3\text{--}4 \text{ nm}$, that will destroy the superconducting correlations. Second, magnetic helicoids exist at magnetic fields $H > 1.5 \text{ T}$ while noncollinear magnetization switches to collinear magnetization in multilayer structures consisting of alternating ferromagnetic layers when field strengths are equal to several hundreds of thousands oersted, with coercive force being the working value of field. Third, the quality of interface between Nb and rare earth elements is higher than that of the interface between Nb and transition metals [7,8]. The disadvantage of the second type systems is complicated penetration of superconducting correlations into thick helimagnetic films followed by their destruction by the exchange field. Better systems are S/F/S systems where the magnetic layer thickness is lower than the correlation superconductivity length in the ferromagnetic material and superconducting correlations fully penetrate into the magnetic layers clamped by the superconducting layers [17].

2. Low-temperature measurements of [Dy(6 nm)/Ho(6 nm)] superlattice

In [9], periodic $\text{Al}_2\text{O}_3(1\bar{1}02)/\text{Nb}(40 \text{ nm})/[\text{Dy}(6 \text{ nm})/\text{Ho}(6 \text{ nm})]_{34}/\text{Nb}(10 \text{ nm})$ heterostructure was studied using polarized neutron reflectometry in REMUR reflectometer of IBR-2 reactor. The study includes more detailed review of low-temperature measurements obtained for this structure at a temperature below $T_c(\text{Nb})$. In [12], it is shown that interface in such systems are characterized by rms roughness amplitude in the amount of five to six atomic monolayers. Note that according to [7,8], good transparent interfaces required for proximity effects to occur are characterized by a roughness amplitude of max. 1.5 nm. Nb layer on the surface serves as protection for the structure against degradation and oxidation. Thin Nb films may exhibit superconducting properties beginning from thicknesses more than 10 nm. But since the 2–3 nm surface of the produced Nb(10 nm) layer is oxide that does not have superconducting properties, the protective Nb layer is suggested to be not superconducting, because the pure Nb thickness is lower than 10 nm.

Neutron measurements of the periodic [Dy(6 nm)/Ho(6 nm)]₃₄ structure were performed using REMUR time-of-flight polarized neutron reflectometer placed in the 8th channel of IBR-2 reactor [18]. The measurements were carried out at a glancing angle of the neutron beam on the sample of $\theta = 19.1 \text{ mrad}$ in the neutron wavelength range of $\lambda_n = 1\text{--}10 \text{ \AA}$. Figure 1 shows the dependence proportional to the magnetic moment of the difference of specular reflection coefficients of neutrons $S = R_+ - R_-$. The data is given for the first-order Bragg peak obtained on the superlattice period. The sample was cooled in magnetic field $H = 1 \text{ kOe}$, measurement was carried out in the same field. It can be seen that S grows with the decreasing temperature indicating that the helimagnetic ordering transforms into the fan-shaped ordering, because collinear component of magnetization grows. But at $T = 1.5 \text{ K} < T_c(\text{Nb})$, inverse behavior is observed, i.e. decreasing S , which indicates that the helimagnetic phase is recovered from the fan-shaped phase. This behavior is associated with the fact that the helimagnetic phase is energetically more advantageous for the existence of superconducting correlations. Integral macroscopic value of magnetic induction in the helimagnetic material is equal to zero, while for magnetic material with fan-shaped magnetic ordering, such value is not equal to zero. It is obvious that the former is more advantageous for superconducting correlations, therefore, magnetic ordering adjustment takes place in magnetic layers. This mechanism is equivalent to that described in [2,3,19,20], where a conclusion is made that one of signs of effect of a superconductor contacting with ferromagnetic material is formation of a special domain structure (crypto-ferromagnetic state) in the ferromagnetic material, where the size of domains d is in the vicinity of the superconducting correlation length in ferromagnetic material $\xi_F \approx 1\text{--}10 \text{ nm}$. Note that the observed effect

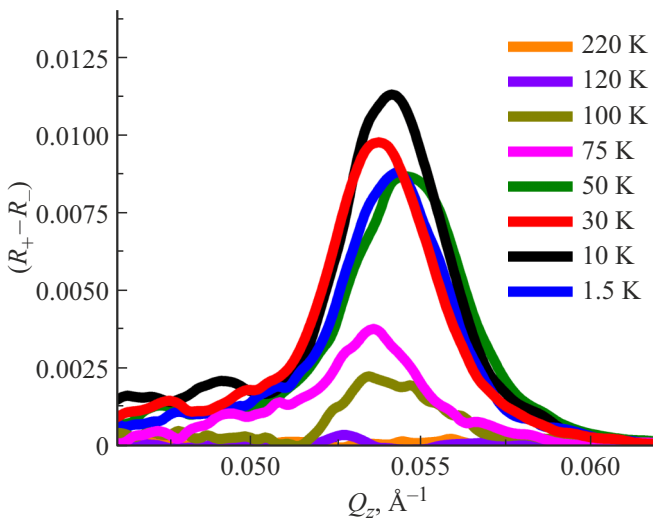


Figure 1. Difference of specular reflection coefficients of neutrons obtained at various temperatures in the magnetic field $H = 1$ kOe.

is high enough, which indicates its long-range coverage typical for generation of spin-triplet correlations. Singlet and triplet correlations in the superconductor vary on the superconducting coherence length which is about $\xi \approx 12$ nm in Nb. Long-range correlations penetrate into the helimagnet to a length defined by the length of long-range correlations which is inversely proportional to temperature and by the magnetic spiral period, which follows from the characteristic equation solution for wave vectors of the Usadel equation solutions in a „dirty“ case. Let us estimate the depth of superconducting correlations into the magnetic layers. Figure 1 shows that the magnetic moment of the structure $M \sim S$ decreases by $\approx 20\%$ in transition from $T = 10$ K to $T = 1.5$ K. Assume that the superconductivity effect, therefore, occurs only at 20% of the thickness of the whole magnetic structure $20\% \cdot 2 \cdot 6 \cdot 34 \approx 80$ nm. According to [9–11], assume the magnetic helicoid period equal to ≈ 3 nm. Then, the effect of long-range superconducting correlations occurs to the depth equal to $80/3 \approx 27$ periods of the magnetic spiral. Note that other mechanisms explaining this phenomenon may include: Meissner shielding of scattering fields by the superconductor, magnetostatic interaction with vortices in the superconductor, shielding of magnetization induced in the multilayer structure by superconductivity. Additional experimental measurements and their review are required. Small shift in Q of dependences shown in Figure 1 is associated with the accuracy of glancing angle of the neutron beam. It may be suggested that at $T > 10$ K helimagnetic ordering transform into fan-shaped ordering when the structure is cooled down, because the collinear component of magnetization grows, which corresponds to transition to ferromagnetic state for bulk Dy and Ho, magnetic state variation at $T = 1.5$ K $< T_c$ (Nb) is associated with the superconductivity effect.

3. Structural properties of $[\text{Nb}(25 \text{ nm})/\text{Dy}(d_F)]$ and $[\text{Nb}(25 \text{ nm})/\text{Ho}(d_F)]$ superlattices

In the system described in Section 2, only the buffer layer Nb(40 nm) is superconducting. Better systems were prepared for the investigation of superconductivity effect on helimagnetic ordering. The structures are superlattices with alternating F and S layers: $\text{Al}_2\text{O}_3(1\bar{1}02)/[\text{Nb}(25 \text{ nm})/\text{RE}(d_F)]_{12}/\text{Nb}(5 \text{ nm})$, where RE = Dy, Ho, $d_f = 2, 4, 6$ nm, thus, structures with magnetic layer thicknesses both lower and higher than the period of magnetic helicoid $d_h \sim 3\text{--}4$ nm were prepared. The structures were produced by magnetron sputtering using ULVAC-MPS-4000-C6 unit in the Institute of Metal Physics of the Ural Branch of the Russian Academy of Sciences according to the procedure described in [9]. $(1\bar{1}02)\text{Al}_2\text{O}_3$ single-crystal was used as a substrate. To protect the structure against oxidation, a Nb(5 nm) layer was sputtered on top of the structure. These structures were qualified.

$[\text{Nb}(25 \text{ nm})/\text{RE}(d_F)]_{12}$ structures were studied on EMPYRIAN (Malvern PANalytical) X-ray diffractometer in geometry $\theta\text{--}2\theta$ using $\text{CuK}\alpha$ radiation with wavelength $\lambda = 1.54 \text{ \AA}$. Characterization of periodic heterostructures was carried out by plotting specular reflection curves, then multilayer system was selected in order to determine the scattering length density (SLD) profile. angle of incidence varied from 0.12 to 1.75° , which corresponded to the scattering vectors $q_z = 0.017\text{--}0.25 \text{ \AA}^{-1}$. Figure 2 shows dependences of the specular reflection coefficient of X-ray beams for samples with various rare earth elements as F layer as well as with various thicknesses of F layer itself. Reflectometry curves were processed

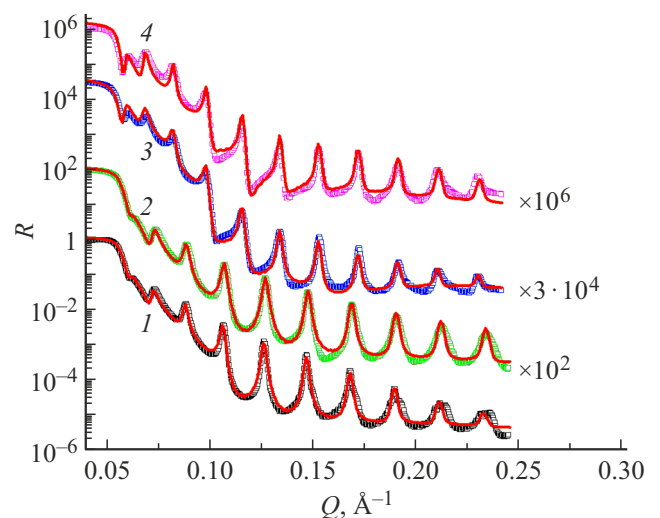


Figure 2. Specular reflection coefficient of X-ray beams for structures: 1 — $[\text{Nb}(25 \text{ nm})/\text{Dy}(2 \text{ nm})]_{12}$, 2 — $[\text{Nb}(25 \text{ nm})/\text{Ho}(2 \text{ nm})]_{12}$, 3 — $[\text{Nb}(25 \text{ nm})/\text{Dy}(6 \text{ nm})]_{12}$, 4 — $[\text{Nb}(25 \text{ nm})/\text{Ho}(6 \text{ nm})]_{12}$. Experimental dependences are shown by dots, theoretical calculation is shown in red color.

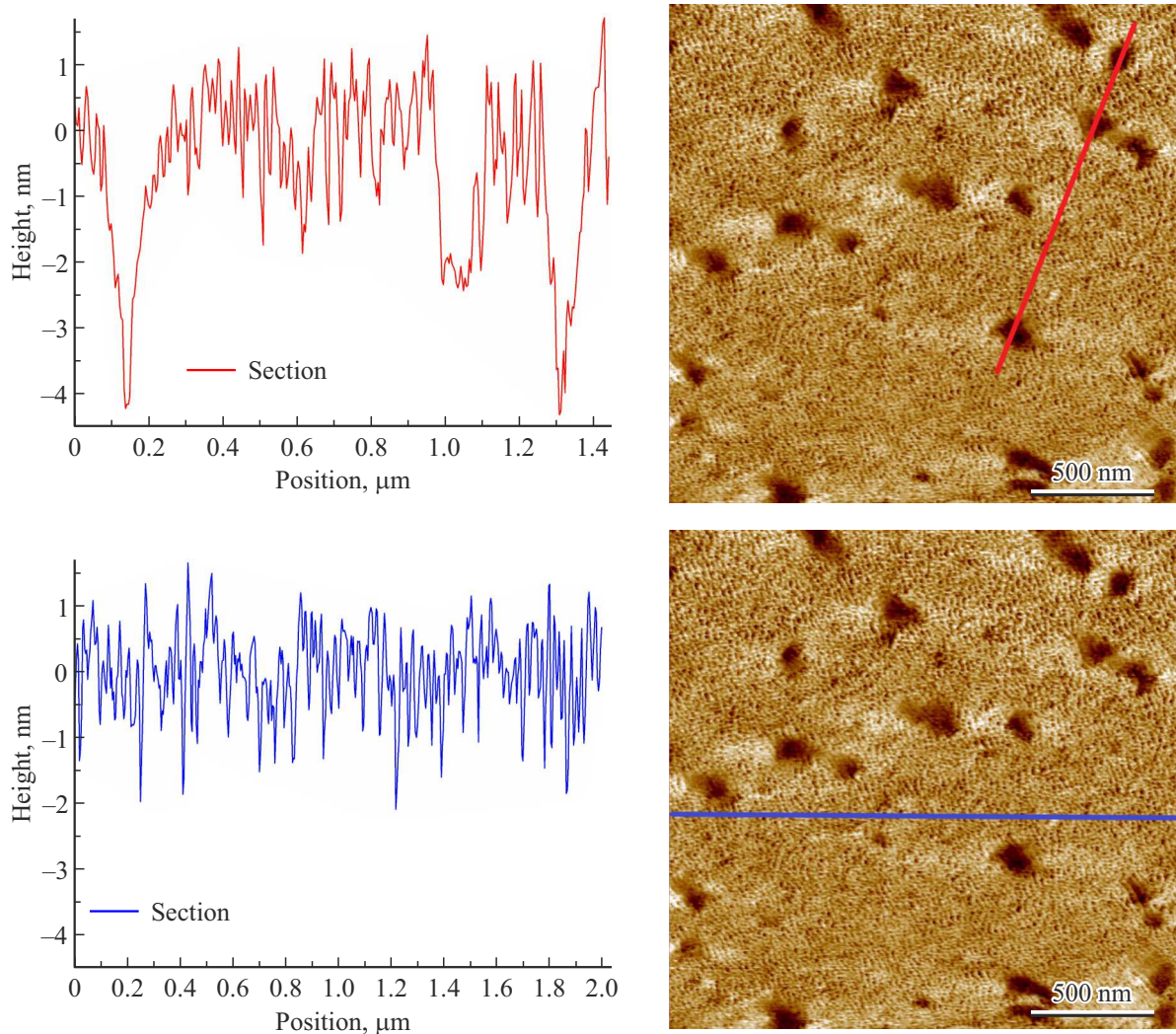


Figure 3. Linear vertical profiles of the surface Nb layer of the section containing pores (upper edge) and smooth section (lower edge).

according to the Parratt formalism using Motofit package for IGOR PRO software [21]. Data processing findings showed that the Nb layer thicknesses differ by not more than 1 nm with respect to the nominal value and the calculated SLD for Nb is very close to the tabular value ($64 \cdot 10^{-6} \text{ \AA}^{-2}$). For Dy or Ho layers, the thicknesses are also close to the nominal values, however, the calculated SLD of these layers is much higher than the tabular value ($50.1 \cdot 10^{-6} \text{ \AA}^{-2}$ and $46.5 \cdot 10^{-6} \text{ \AA}^{-2}$, respectively), which may indicate the presence of rather thick intermediate layers in case of $d_F = 6 \text{ nm}$, and the absence of pure F layer in case of $d_F = 2 \text{ nm}$. Interlayer boundaries are characterized by the rms roughness amplitude for all layers of $\max. R_q \sim 1.5 \text{ nm}$, however it should be noted that roughness for the surface Nb layer is high for all samples and is equal to 2.5–3 nm. Thus, high repeatability of Dy/Nb and Ho/Nb bilayers was shown, while the actual layer thickness differs from the nominal values by max. 5%. Data demonstrates homogeneity of these systems at the Nb/Gd structure level [7].

The atomic-force microscopy method was used to analyze the surface Nb (5 nm) layer to check the quality and compare with the X-ray reflectometry data. Surface profile was analyzed using NTEGRA (NM MDT Spectrum Instruments) atomic-force microscopy (AFM) — in semi-contact („tapping“ mode). HA_{HR} cantilever (Si probe, $R < 10 \text{ nm}$, $k = 34 \text{ N/m}$, $\nu = 380 \text{ kHz}$) was used as a probe. Images were obtained as 512×512 , linear scanning rate was 0.2–0.3 Hz for each line, scan area was $2 \times 2 \mu\text{m}$. Vertical profile of the Nb layer surface was recorded and looked like a surface with large number of through pores and „ripple“ typical of Nb layers [22]. Further processing of the surface images showed that these pores with a mean size of 89 nm run through the Nb layer and their typical depth is 5.2 nm, which corresponds to the thickness of the layer itself (Figure 3). RMS roughness of the pore-free surface is $S_q = 0.65 \text{ nm}$, which is lower than the values of simulated reflectometry curves. Thus, high effective roughness of the Nb layer in the reflectometry method is associated with the presence of a lot of pores on the surface.

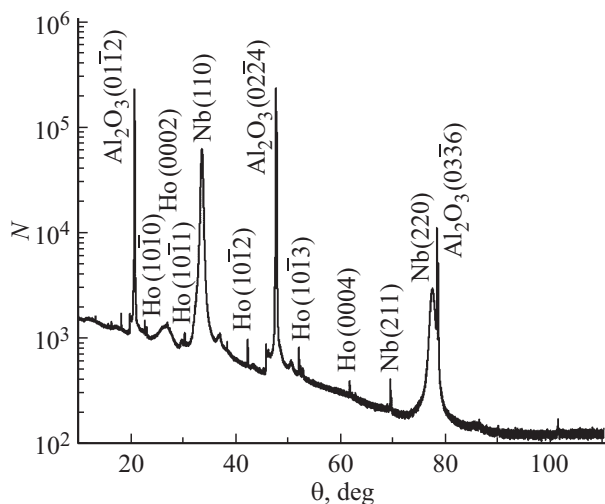


Figure 4. X-ray image for $[\text{Nb}(25 \text{ nm})/\text{Ho}(4 \text{ nm})]_{12}$ structure made in geometry $\theta-2\theta$, diffraction peaks are indicated.

X-ray diffraction measurements were carried out in geometry $\theta-2\theta$, the incidence angle varied from 10 to 110° . Figure 4 shows the X-ray image for structure $d_F(\text{Ho}) = 4 \text{ nm}$. The indicated diffraction peaks are similar to the results provided in [10]. Therefore, it was suggested by analogy that Nb, Ho, Dy lattice constants correspond to bulk crystals. Crystalline structure orientation of Dy layers correspond to the helicoid axis orientation perpendicular to the structure plane.

4. Conclusions

Possibility of control over the magnetic ordering of helimagnet using superconductivity was demonstrated. It was shown that in the periodic Dy/Ho structure sputtered on the superconducting Nb buffer, fan-shaped magnetic ordering transforms into helimagnetic ordering at a temperature below $T_c(\text{Nb})$. Structures with alternating superconductor and rare-earth helimagnetic layers were offered and produced for the investigation of magnetic proximity effects. X-ray diffraction and microscopic studies have shown high quality of structures meeting the investigation requirements. Layer thicknesses differ by max. 5% with respect to the nominal value, rms roughness amplitude was max. 1.5 nm, interlayer boundaries may be defined as the boundaries with high smoothness. High quality of the produced structures will allow to study the influence of superconductivity on helimagnetic ordering, in particular on the helicoid period.

Funding

The study was supported by RSF grant No. 22-72-00116. The samples were synthesized in the Center for Collective Use of the Institute of Metal Physics, Ural Branch, Russian Academy of Sciences, under the State Assignment of the Ministry of Science and Higher Education of the Russian Federation (topic „Spin“ No. AAAA-A18-118020290104-2).

This study was funded by the scientific foundation of the National Research University Higher School of Economics and the Ministry of Science and Higher Education of the Russian Federation, Agreement No. 075-15-2021-1353.

Conflict of interest

The authors declare that they have no conflict of interest.

References

- [1] S. Mironov, A.S. Mel'nikov, A. Buzdin. *Appl. Phys. Lett.* **113**, 022601 (2018).
- [2] A.I. Buzdin. *Rev. Mod. Phys.* **77**, 3, 935 (2005).
- [3] P.W. Anderson, H. Suhl. *Phys. Rev.* **116**, 898 (1959).
- [4] Yu.V. Nikitenko, V.D. Zhaketov. *Phys. Part. Nucl.* **53**, 6, 1089 (2022).
- [5] V.D. Zhaketov, Yu.V. Nikitenko, Yu.N. Khaidukov, O.V. Skryabina, A. Csik, M.M. Borisov, E.Kh. Mukhamedzhanov, S.N. Vdovichev, E.I. Litvinenko, A.V. Petrenko, A.V. Churakov. *J. Exp. Theor. Phys.* **129**, 2, 258 (2019).
- [6] V.D. Zhaketov, Yu.V. Nikitenko, F. Radu, A.V. Petrenko, A. Csik, M.M. Borisov, E.Kh. Mukhamedzhanov, V.L. Aksenov. *J. Exp. Theor. Phys.* **124**, 1, 114 (2017).
- [7] Yu.N. Khaydukov, E.A. Kravtsov, V.D. Zhaketov, V.V. Proglyado, G. Kim, Yu.V. Nikitenko, T. Keller, V.V. Ustinov, V.L. Aksenov, B. Keimer. *Phys. Rev. B* **99**, 140503(R) (2019).
- [8] Yu.N. Khaydukov, A.S. Vasenko, E.A. Kravtsov, V.D. Zhaketov, V.D. Zhaketov, A. Csik, Yu.V. Nikitenko, A.V. Petrenko, T. Keller, A.A. Golubov, M.Yu. Kupriyanov, V.V. Ustinov, V.L. Aksenov, B. Keimer. *Phys. Rev. B* **97**, 144511 (2018).
- [9] D.I. Devyaterikov, E.A. Kravtsov, V.V. Proglyado, V.D. Zhaketov, Yu.V. Nikitenko. *J. Surf. Investigation* **16**, 5, 839 (2022).
- [10] D.I. Devyaterikov, V.V. Proglyado, V.D. Zhaketov, E.A. Kravtsov, V.V. Ustinov. *Phys. Met. Metallogr.* **122**, 5, 465 (2021).
- [11] D.I. Devyaterikov, E.A. Kravtsov, V.V. Proglyado, V.D. Zhaketov, Yu.V. Nikitenko. *J. Surf. Investigation* **15**, 3, 542 (2021).
- [12] D.I. Devyaterikov, V.O. Vas'kovsky, V.D. Zhaketov, E.A. Kravtsov, M.V. Makarova, V.V. Proglyado, E.A. Stepanova, V.V. Ustinov. *Phys. Met. Metallogr.* **121**, 12, 1127 (2020).
- [13] N.G. Pugach, M.O. Safonchik, V.I. Belotelov, T. Ziman, T. Champel. *Phys. Rev. Appl.* **18**, 5, 054002 (2022).
- [14] V.O. Yagovtsev, N.A. Gusev, N.G. Pugach, M. Eschrig. *Supercond. Sci. Technol.* **34**, 025003 (2021).
- [15] N.G. Pugach, M. Safonchik, T. Champel, M.E. Zhitomirsky, E. Lähderanta, M. Eschrig, C. Lacroix. *Appl. Phys. Lett.* **111**, 162601 (2017).
- [16] Yu, Gu, Gábor B. Halász, J.W.A. Robinson, M.G. Blamire. *Phys. Rev. Lett.* **115**, 067201 (2015).
- [17] N. Klenov, Yu. Khaydukov, S. Bakurskiy, R. Morari, I. Soloviev, V. Boian, T. Keller, M. Kupriyanov, A. Sidorenko, B. Keimer. *Beilstein J. Nanotechnol.* **10**, 833–839 (2019).
- [18] V.L. Aksenov, K.N. Jernenkov, S.V. Kozhevnikov, H. Lauter, V. Lauter-Pasyuk, Yu.V. Nikitenko, A.V. Petrenko. *Communication of the JINR*, D13-2004-47 (2004).
- [19] A.I. Buzdin, L.N. Bulayevsky. *JETP* **89**, 753 (1988)
- [20] F.S. Bergeret, K.B. Efetov, A.I. Larkin. *Phys. Rev. B* **62**, 11872 (2000).
- [21] A. Nelson. *J. Appl. Cryst.* **39**, 273 (2006).
- [22] L.R. Nivedita, A. Haubert, A.K. Battu, C.V. Ramana. *Nanomaterials (Basel)* **10**, 7, 1287 (2020).

Translated by Ego Translating